Role of stationary invariant manifolds in the spatiotemporal dynamics of a nonlinear-wave system of finite extension: Application to polarization attraction in optical fibers

K. Hamraoui, M. Guasoni, A. Picozzi, E. Assémat, H. R. Jauslin, and D. Sugny*

Laboratoire Interdisciplinaire Carnot de Bourgogne (ICB), UMR 6303 CNRS-Université Bourgogne Franche Comté, 9 Av. A. Savary, BP 47 870, F-21078 Dijon, France

(Received 15 January 2016; published 24 May 2016)

The study of the spatiotemporal dynamics of two counterpropagating beams in optical fibers has recently been the subject of a growing renewed interest. This system has been shown to exhibit a phenomenon of polarization attraction which can be used to achieve a complete polarization of an initially unpolarized beam, almost without any loss of energy. In previous works, a theoretical description of this phenomenon has been developed in the particular case where the underlying stationary system exhibits the important property of integrability. Our aim here is to provide a generalization of the theoretical description to nonintegrable stationary systems. The analysis reveals that the spatiotemporal dynamics of the system relaxes towards a stationary trajectory whose geometric structure is revealed by the stable and unstable manifolds of some singular fixed points of the stationary system. We illustrate the theory by considering the representative and concrete example of a weakly birefringent optical fiber system.

DOI: 10.1103/PhysRevA.93.053830

I. INTRODUCTION

Recent theoretical and computational studies of the spatiotemporal dynamics of counterpropagating waves in nonlinear media of finite spatial extension have brought forward the relevance of classical Hamiltonian approaches of the associated stationary dynamical system for the understanding of the system ruled by partial differential equations (PDEs) [1–8]. In particular, under rather general conditions, it has been shown that the wave systems can exhibit a process of relaxation characterized by an evolution towards a stationary state. Such a stationary state can be identified and described through the dynamics of the spatial system, which is governed by a set of ordinary differential equations (ODEs) [3]. So far, most of the works have considered specific cases for which the stationary system is an integrable system, i.e., it has as many constants of motion as degrees of freedom [2,3,9–23]. In this framework, Hamiltonian singularities associated with singular tori [24,25] in the phase space of the stationary system [14,15] allowed us to identify the corresponding "attractors" of the phenomenon of relaxation of the PDE system. More precisely, it has been shown that the PDE system converges exponentially towards a trajectory lying on the singular torus in the limit of an infinite medium; the singular torus thus plays the role of an attractor for the PDE system of infinite degrees of freedom. In this way, singular tori were shown to be the "precursors" of this dynamical process of relaxation for a series of PDE systems, such as the three- and four-wave interaction equations, or the Thirring-like model which is known to describe, e.g., the dynamics of nonlinear waves in periodic lattices [14,15].

This phenomenon of spatiotemporal relaxation has been the subject of a recent growing interest in the particular context of nonlinear fiber optics, from both the theoretical and experimental points of view [3]. In this framework, the relaxation process finds an important application, namely, the possibility to achieve an all-optical control of the state of polarization (SOP) of a forward wave by adjusting the injected SOP of the backward wave [2,3,9,11–23]. This phenomenon of "polarization attraction" has been demonstrated in many different types of optical fiber systems, such as isotropic fibers, spun fibers, and highly birefringent or even randomly birefringent fibers used in optical telecommunications. In addition, the effect of polarization attraction has been also demonstrated in the absence of the injected backward wave—the forward beam interacting in this case with its own counterpropagating replica produced by means of a backreflection Bragg mirror at the fiber output [26–28]. Besides its fundamental interest, we would like to stress the importance of this effect from the applicative point of view. Polarization attraction can be used to achieve a complete repolarization of an initially unpolarized signal beam with almost 100% efficiency, a feature which contrasts with standard polarizers that unavoidably waste 50% of the incoming light [29,30]. This effect is particularly appealing since it finds natural important applications as a polarization device in optical telecommunication transmission lines [20,21,31].

Most of the theoretical studies of polarization attraction discussed above have a common important property: the underlying stationary ODE system is an integrable Hamiltonian system. This is indeed a key property required by the applicability of the geometric approach discussed above, since a proper characterization of the singularities of the stationary system (singular tori) can only be accomplished for integrable systems. Our aim in this article is to extend the geometric approach of the phenomenon of polarization attraction to more general systems where the associated stationary ODE does not need to satisfy the severe constraint of integrability. We address this issue by considering the representative example of an optical fiber with a weak birefringence [8,32], a property which is known to break the integrability of the associated stationary ODE system [8]. Furthermore, this issue is typically relevant for optical fibers that are not short enough to be considered as isotropic, i.e., in fibers whose length scale is of the same order as the birefringence beat length, so that birefringence can strongly impact the polarization dynamics. The numerical simulations reveal that the process of polarization attraction can still occur efficiently when the birefringence is a perturbative effect. The theoretical analysis remarkably shows that the

*dominique.sugny@u-bourgogne.fr

invariant manifolds (stable and unstable manifolds) of some specific fixed points of the stationary system [33,34] play an attracting role for the PDE system, in a way analogous to the role played by singular tori in the integrable case. In addition, we show that the geometric structure of the final state of the spatiotemporal system can be revealed and understood through the analysis of the dynamics on these invariant sets. This work then also reveals the unexpected fundamental role of attractors that play the invariant manifolds of the associated ODE system in the whole spatiotemporal PDE system.

The remainder of this article is organized as follows. The principal properties of the model are summarized in Sec. II. A geometric analysis of the stationary ODE system and of its fixed points is the focus of Sec. III. The numerical results are presented in Sec. IV. A conclusion and prospective views are given in Sec. V. Some technical computations are reported in Appendixes A and B.

II. THE MODEL SYSTEM

We consider the one-dimensional counterpropagating configuration of four-wave interaction. This model has been widely used in the past to describe counterpropagating beams in optical fiber systems [1–3,9–21,26–28]. In this paper we consider the specific case of the polarization dynamics in an optical fiber with a weak birefringence, because this latter property will be shown to break the integrability of the corresponding stationary ODE system. We recall that birefringence in optical fibers refers to the dependence of the refractive index on light polarization. It is usually quantified by the maximum difference $\Delta n = n_S - n_F$ between the refractive indices of the principal axes of the fiber, where n_F and n_S are the indices along the fast and slow birefringence axes, respectively. Propagation constants of light traveling along such two axes read, respectively, $k_F = 2\pi n_F/\lambda$ and $k_S = 2\pi n_S/\lambda$, λ being the light wavelength. Therefore the electric field components along the birefringence axes experience a phase shift of 2π every beat length $L_b = \lambda/\Delta n$, which also defines the length scale of the linear coupling between the rectilinear polarization components. Here we address the case in which L_b is of the same order as the fiber length, which in turn is much shorter than the typical correlation length L_c of random birefringence fluctuations that are known to impact kilometers-long telecommunication fibers (see Ref. [21]). Therefore, the birefringence considered in this work is assumed to be fully deterministic. For completeness, we briefly sketch in Appendix A the derivation of the model from basic propagation equations in optical fiber systems.

It proves convenient to use the Stokes formalism, in which the dynamics of polarization of the counterpropagating beams can be shown to be governed by the following equations (see Appendix A):

$$\frac{\partial \vec{S}}{\partial t} + \frac{\partial \vec{S}}{\partial z} = \vec{S} \times (\mathcal{I}\vec{S}) + 2\vec{S} \times (\mathcal{I}\vec{J}) + \Delta \vec{S} \times \vec{e}_1, \quad (1)$$

$$\frac{\partial \vec{J}}{\partial t} - \frac{\partial \vec{J}}{\partial z} = \vec{J} \times (\mathcal{I}\vec{J}) + 2\vec{J} \times (\mathcal{I}\vec{S}) + \Delta \vec{J} \times \vec{e}_1, \quad (2)$$

where the Stokes vectors $\vec{S} = (S_1, S_2, S_3)$ and $\vec{J} = (J_1, J_2, J_3)$ describe, respectively, the SOPs of the forward and backward waves on the Poincaré sphere. The vector $\vec{e}_1$ denotes the unit vector along the 1 direction, and $\Delta = k_S - k_F$ is the birefringence parameter defined above. The diagonal matrix $\mathcal{I}$ reads $\mathcal{I} = \mathrm{diag}(-1,-1,0)$. With these notations, the circular SOPs are located on the 3 axis. We also introduce the radii S_0 and J_0 of the forward and backward spheres, which are directly related to the conserved signal and pump powers [2]. For convenience, Eqs. (1) and (2) have been normalized with respect to the nonlinear interaction time $\tau_0 = 1/(\gamma S_0)$ and length $\Lambda_0 = v\tau_0$, where γ is the nonlinear coefficient and v the group velocity of the waves. Note that the physical variables can be recovered in standard units through the transformations $t \to t\tau_0$, $z \to z\Lambda_0$ and $(\vec{S}, \vec{J}) \to (\vec{S}, \vec{J})S_0$. We remark that because of the counterpropagating configuration, the boundary conditions are defined by the signal and pump SOPs $\vec{S}(z = 0)$ and $\vec{J}(z = L)$ at the opposite fiber ends, respectively, at $(z = 0)$ and at $(z = L)$, where L denotes the normalized fiber length. For such fixed boundary conditions, the powers S_0 and J_0 are conserved during the propagation of the waves. For the sake of simplicity, in the following we consider the case where the counterpropagating beams have equal powers, i.e., $S_0 = J_0 = 1$ with our normalization. The same analysis can easily be extended to the case of different powers.

III. GEOMETRICAL ANALYSIS OF THE STATIONARY STATES

We consider the stationary system of equations by dropping the time derivatives in Eqs. (1) and (2):

$$\begin{aligned} \dot{S}_1 &= S_3 S_2 + 2S_3 J_2 \\ \dot{S}_2 &= -S_3 S_1 - 2S_3 J_1 + \Delta S_3 \\ \dot{S}_3 &= 2J_1 S_2 - 2S_1 J_2 - \Delta S_2 \end{aligned} \quad (3)$$

and

$$\begin{aligned} \dot{J}_1 &= -J_3 J_2 - 2J_3 S_2 \\ \dot{J}_2 &= J_3 J_1 + 2J_3 S_1 - \Delta J_3 \\ \dot{J}_3 &= 2J_1 S_2 - 2S_1 J_2 + \Delta J_2 \end{aligned} \quad (4)$$

where the dots denote derivatives with respect to the spatial variable z. These equations have a Hamiltonian structure leading to the following Poisson brackets [24,33]:

$$\{S_1, S_2\} = S_3; \ \{J_1, J_2\} = -J_3. \quad (5)$$

The other relations are obtained by a circular permutation of the indices. The equations admit a single constant of motion, the Hamiltonian of the system:

$$H = 2(S_1 J_1 + S_2 J_2) - \tfrac{1}{2}\left(S_3^2 + J_3^2\right) - \Delta(S_1 + J_1). \quad (6)$$

It is important to note that birefringence [i.e., the term $\Delta(S_1 + J_1)$], breaks the integrability of the system. In the limit of a vanishing birefringence, $\Delta = 0$, the stationary system admits a second constant of motion $K = S_3 - J_3$, which reestablishes integrability.

A. Relation with the approach developed for the integrable limit

As mentioned in the Introduction, previous geometric investigations of these types of dynamical systems were

completely based on the integrability of the stationary system. In this case, the Liouville-Arnold theorem states that all the trajectories of the system lie on a torus. The tori are in general regular, but some of them can be singular [24]. An example is given by a pinched torus, which is a regular torus whose radius has been pinched to zero in one point. A pinched torus can also be defined as the union of the stable and unstable manifolds [34] of the pinched point, which is a fixed point for the dynamical system. More generally, the singular tori can also be viewed as the higher-dimensional generalization of the separatrices when the Hamiltonian system is integrable [2,24]. The relevance of these mathematical structures has been only recently recognized in physics [25], and particularly for the understanding and the description of the qualitative properties of the dynamics of PDE systems [14,15].

In the case investigated in this paper, the integrable system, i.e., the one for $\Delta = 0$, has a doubly pinched torus characterized by the constants $H = -1$ and $K = 0$. We refer the reader to Refs. [14,15] for a complete geometrical description of this system and to Appendix B for a detailed computation of its stable and unstable manifolds. This torus has two fixed points, the two pinched points, of coordinates $S_3 = \pm 1$ (forward-right or left-circular polarizations) and $J_3 = \pm 1$ (backward-right or left-circular polarizations). When the parameter Δ is different from 0, the integrability is lost and most of the tori, and in particular the singular one, are destroyed [35,36]. *However, the singularity does not completely disappear, in the sense that some of its dynamical features are still preserved. In particular, in the presence of a weak perturbation that breaks the integrability, the fixed points are preserved.* This remark is at the origin of the geometric analysis which is aimed at revealing the crucial role of the fixed points and their corresponding stable and unstable manifolds in the spatiotemporal dynamics of the nonlinear-wave system.

B. Stationary fixed points and line of polarization attraction

The first step of the analysis consists in studying the nature of the fixed points of the stationary system given by the relations

$$\begin{aligned} -S_3S_1 - 2S_3J_1 + \Delta S_3 &= 0 \\ J_3J_1 + 2J_3S_1 - \Delta J_3 &= 0. \end{aligned} \tag{7}$$

For $\Delta = 0$, the two fixed points of interest are the ones of the doubly pinched torus, i.e., the points of coordinates $(S_3 = 1, J_3 = 1)$ and $(S_3 = -1, J_3 = -1)$. In the case $\Delta \neq 0$, we first determine the position of the new fixed points. We consider a perturbation around the standard solution $S_3 = \pm 1$ and $J_3 = \pm 1$. We deduce from the stationary equations that $S_2 + 2J_2 = 0$ and $J_2 + 2S_2 = 0$, which leads to $S_2 = J_2 = 0$. We arrive at

$$J_3^2 S_3^2 (J_1 - S_1) = 0, \tag{8}$$

which gives $J_1 = S_1$ and $J_3 = \pm S_3$. We finally get that

$$S_1 = J_1 = \frac{\Delta}{3}; \;\; S_3 = \pm\sqrt{1 - \Delta^2/9}; \;\; J_3 = \pm\sqrt{1 - \Delta^2/9}, \tag{9}$$

and $S_2 = J_2 = 0$. The two fixed points for which S_3 and J_3 have different signs are stable (elliptic) and the ones with equal signs are unstable (hyperbolic) and correspond to the deformed pinched torus. Note that in the limit $\Delta = 0$, these fixed points correspond to the circular SOPs (the poles of the Poincaré sphere). For such fixed points, the value of the stationary Hamiltonian is given by $H = -1 - \frac{\Delta^2}{3}$. Due to the nonintegrability, only one constant of motion, the Hamiltonian, is preserved in the stationary dynamics. The *singular trajectories* of the Hamiltonian stationary system lie on the surface defined by $H = -1 - \Delta^2/3$. This constraint on the value of H leads to a line in the $\vec{S}$- Poincaré sphere at $z = L$, which is completely given by the boundary value of the pump SOP, $\vec{J}(z = L)$. This line is defined implicitly by the following equation:

$$\begin{aligned} -1 - \frac{\Delta^2}{3} &= 2[S_1 J_1(L) + S_2 J_2(L)] \\ &\quad - \frac{1}{2}\left[S_3^2 + J_3(L)^2\right] - \Delta[S_1 + J_1(L)], \end{aligned} \tag{10}$$

where we recall that the value of $\vec{J}(L)$ is specified by the boundary conditions. For instance, in the case where the injected pump beam has a circular SOP, i.e., $J_3(L) = 1$, we get

$$S_3^2 + 2\Delta S_1 = 1 + 2\frac{\Delta^2}{3}. \tag{11}$$

In the case $J_2(L) = 1$, we obtain

$$2S_2 - \frac{1}{2}S_3^2 - \Delta S_1 = -1 - \frac{\Delta^2}{3}. \tag{12}$$

Figure 1 displays an example of this line for a "generic" pump SOP, $\vec{J}(L) = (1/\sqrt{3}, 1/\sqrt{3}, 1/\sqrt{3})$.

Note that, in the integrable case ($\Delta = 0$), the second constant of the motion K defines another line in the $\vec{S}$-Poincaré sphere. The intersection of the two lines is a point which completely defines the process of polarization attraction [2,16]. In the nonintegrable case ($\Delta \neq 0$), a supplementary work is required to completely determine the attraction phenomenon.

IV. SPATIOTEMPORAL SIMULATIONS OF POLARIZATION ATTRACTION

A. Numerical results

In this section, we investigate the relaxation and the attraction effects in an optical fiber with a weak birefringence through intensive numerical simulations of the spatiotemporal dynamics governed by Eqs. (1) and (2). To assess the influence of the birefringence, it is important to compare the length of the fiber with the characteristic length associated with the birefringence effect. In dimensionless units these two length scales respectively read L and $L_B = 2\pi/\Delta$. The corresponding ratio $\rho = L_B/L$ is then related to the birefringence parameter by $\Delta = 2\pi/(\rho L)$. The impact of birefringence becomes important as ρ becomes small. Note that the parameter ρ can easily be determined experimentally—it is typically of the order of unity for a fiber length of a few meters.

In all the cases investigated below, 64 different initial states of polarization of the signal $\vec{S}(z = 0, t)$ have been uniformly distributed over the surface of the Poincaré sphere (see Fig. 1). On the other hand, the pump SOP is fixed, $\vec{J}(z = L)$. The boundary conditions are kept fixed in time,

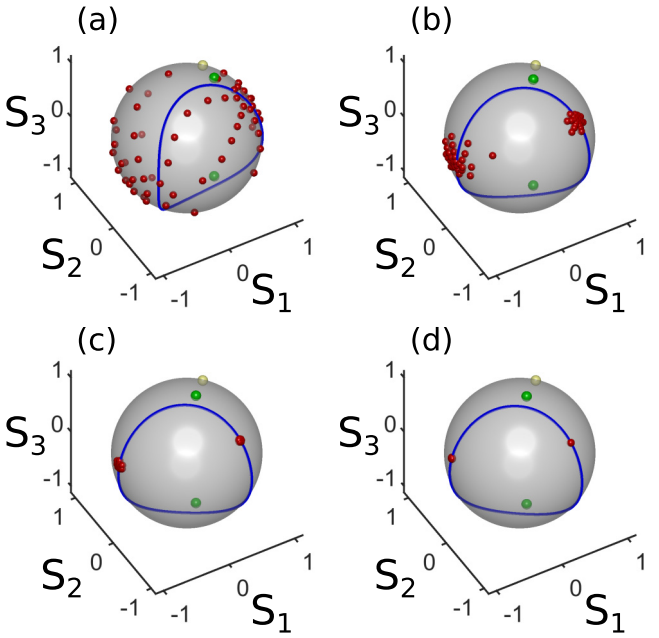

FIG. 1. Results of the numerical simulations of the spatiotemporal PDE system on the Poincaré sphere with $\rho = 5$. The red dots denote the states of the signal at $z = L$ when the stationary dynamics is reached. The fiber lengths are set to $L = 1$ (a), $L = 2$ (b), $L = 3$ (c), and $L = 4$ (d). The yellow dot displays the boundary condition of the pump SOP, $\vec{J}(L) = (1/\sqrt{3},1/\sqrt{3},1/\sqrt{3})$, and the green dots the fixed points of the stationary ODE system. The blue solid line depicts the curve of points (line of polarization attraction) with the same energy H as the fixed point (see Sec. III for details). We recall that $S_3 = \pm 1$ denotes the right or left circular polarization states. The different quantities are dimensionless.

$\vec{S}(z = 0,t)$ and $\vec{J}(z = L,t)$, and Fig. 2 reports the stationary states of the signal SOP $\vec{S}(z)$ reached after some sufficiently long spatiotemporal transient (see [2] for more details on the computation procedure). Typical results of the simulations are reported in Figs. 1 and 2 for different values of the normalized fiber length, L. Figure 2 displays the spatial profile of the stationary state $S_3(z)$ that the system has reached after a spatiotemporal transient relaxation process. Different values of the fiber length have been considered in the different panels of Fig. 2. Figure 1 reports the corresponding output signal SOPs, $\vec{S}(z = L)$, on the surface of the Poincaré sphere. In these first series of numerical computations, the value of the parameter ρ has been kept fixed. We observe that the process of polarization attraction is more efficient as the fiber length L is increased. Two attracting points, $\vec{S}(z = L)$, exist according to the initial SOP of the signal. It seems therefore that each attracting point has a different basin of attraction. It is important to note that, before being attracted, Fig. 2 clearly shows that the signal passes through a point which is located close to either the north pole or the south pole of the Poincaré sphere.

As illustrated by Figs. 1 and 2, the efficiency of the attraction process increases as the fiber length L is increased, as revealed by the reduction of the spreading of the signal SOPs at the fiber output $\vec{S}(z = L)$. Figure 1 shows that this latter point of attraction belongs to the line of polarization attraction predicted by the theoretical analysis in Sec. III B.

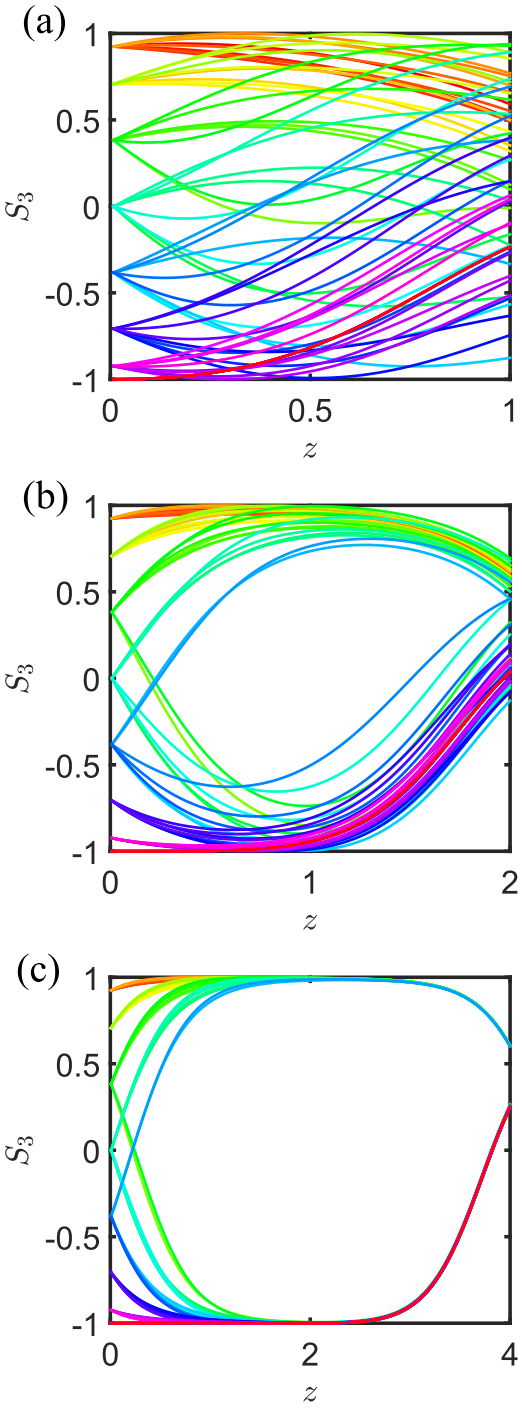

FIG. 2. Stationary solutions that the PDE system governed by Eqs. (1) and (2) reaches after a transient spatiotemporal relaxation process. The figure illustrates the particular coordinate S_3 vs z. The fiber lengths are set to $L = 1$ (a), $L = 2$ (b), $L = 4$ (c). The parameter ρ is fixed to 5. The boundary condition of the pump SOP is fixed to $\vec{J}(z = L) = (1/\sqrt{3},1/\sqrt{3},1/\sqrt{3})$. 64 different boundary conditions of the signal SOP, $\vec{S}(z = 0)$, are considered (see Fig. 1). We recall that $S_3 = \pm 1$ denotes the right or left circular polarization states. The different quantities are dimensionless.

The reduction of the spreading of the signal SOPs $\vec{S}(L)$ when the fiber length increases constitutes a well-known property of the polarization attraction effect. In the case under consideration, the efficiency of the process can be evaluated

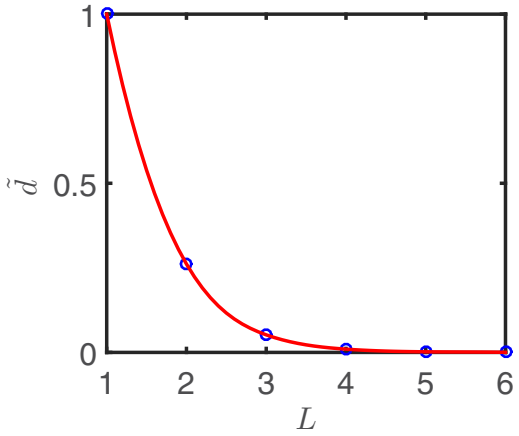

FIG. 3. Evolution of the distance d, defined in Eq. (13), as a function of the fiber length L for the input pump SOP $\vec{J}(z = L) = (1/\sqrt{3}, 1/\sqrt{3}, 1/\sqrt{3})$, while the signal boundary conditions are uniformly distributed on the surface of the Poincaré sphere. The distance is normalized with respect to its value for $L = 1$ [$\tilde{d}(L) = d(L)/d(L = 1)$] to improve the visualization of the convergence toward the singular line of attraction. The parameter ρ is set to 5. When L varies from 1 to 6, the range of variation of Δ is from $2\pi/5$ to $2\pi/30$. The different quantities are dimensionless.

by using a measure of the distance d to the singular line,

$$d(L) = \sum_i \sqrt{(H_i - H_s)^2}, \tag{13}$$

where the index i runs over all the initial SOPs of the signal beam. H_i is the value of the constant of the motion H of the corresponding stationary state i, and H_s is the Hamiltonian of the fixed point of the stationary dynamics. We have performed a systematic numerical study of the attraction process for different fiber lengths L, as illustrated in Fig. 3. The study reveals that the distance rapidly tends to 0 as L increases. Note that this value of the distance to the singular line is already remarkably small for a relatively small value of $L \simeq 6$. The same analysis is conducted in Fig. 4 to evaluate the impact of the birefringence parameter Δ. As could be expected, we observe that the spreading increases as

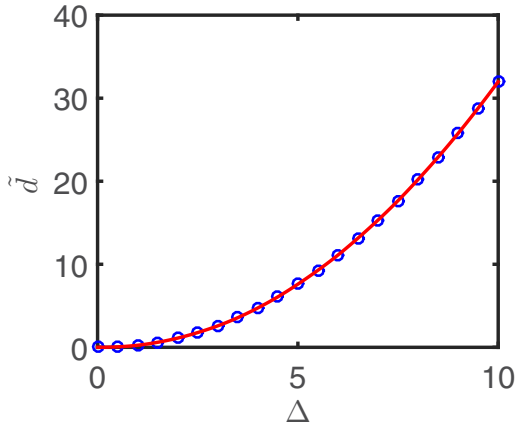

FIG. 4. Same as in Fig. 3, except that now the birefringence parameter Δ is varied while keeping the fiber length constant, $L = 4$.

Δ increases, a feature which clearly reveals the negative impact of the nonintegrable birefringence effect on the phenomenon of polarization attraction.

We conclude this paragraph by remarking that the normalized values of $\rho = 5$ and $L = 4$ may correspond to a propagation regime characterized by the following characteristic length scales: $\hat{L} = 4m$, $\hat{L}_b = 20m$, and $\hat{L}_{nl} = 1m$, with $\hat{L}$, $\hat{L}_b$, and $\hat{L}_{nl}$ the real (dimensional) fiber length, beat length, and nonlinear length, respectively. This regime can be met in practice in a spun fiber, where the underlying fiber spinning process is known to substantially reduce the birefringence strength, and by considering nanosecond pump pulses, whose peak power may reach several tens of Watts, so as to make the nonlinear length as short as a few meters [11]. Also notice that in this short fiber experimental configuration, random fluctuations of birefringence can be usually neglected.

B. Two-stage process of polarization attraction

A detailed analysis of the effect of polarization attraction reveals that it occurs sequentially, in two distinct stages. This becomes apparent when one analyzes the *spatial dependence of the stationary solutions* on the Poincaré sphere representation. The two-stage process is illustrated in Fig. 5 (see also the movie in the Supplemental Material [37]), which reports the trajectory of the 64 SOPs discussed above in Figs. 1 and 2 for different values of the spatial coordinate z. In the first stage [panels (a)–(e) in Fig. 5], we note that the signal SOPs are contracted into the vicinity of one of the two fixed points on the surface of the Poincaré sphere. A basin of attraction can be associated with each fixed point. In a second stage, the signal SOPs evolve together by following essentially the same trajectory (one trajectory for each fixed point) to reach the final point of polarization attraction. As predicted, this point belongs to the attraction line define above in Sec. III B.

On the basis of these numerical observations, we now formulate two conjectures on the dynamics.

Conjecture 1: Under general boundary conditions, the PDE system relaxes towards a stationary solution.

Conjecture 2: In the limit where the length of the medium goes to infinity, the stationary solution lies in the vicinity of the invariant sets of one of the two fixed points. The signal and the pump first approach the fixed point from a trajectory that closely follows the stable manifold, and then they escape from this fixed point to reach the final point of polarization attraction by following a trajectory close to the unstable manifold.

It may appear counterintuitive that unstable manifolds may play a role of attractors in this system. However, let us recall that the invariant set is a structure of the ODE system, while the attraction point is a feature of the PDE dynamics. In this respect, we also note that homoclinic orbits of ODE systems are known to play a crucial role for soliton solutions of the corresponding PDE system.

C. Stable and unstable manifolds

The next step of the geometric study is based on the analysis of the stability of the stationary dynamics with respect to a small perturbation in a neighborhood of the fixed points. For that purpose, we consider a linearization of the dynamical

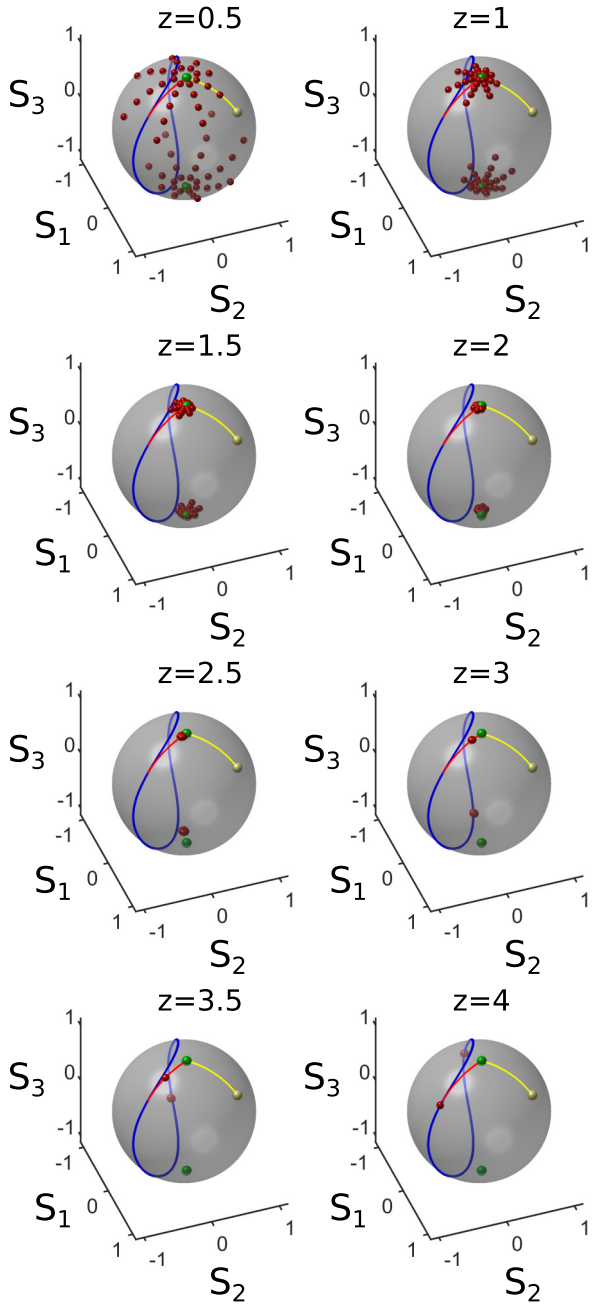

FIG. 5. Sequential Poincaré sphere evolution illustrating the two-stage process of polarization attraction. The initial 64 signal SOPs [red (dark gray) dots] are uniformly distributed on the Poincaré sphere (from left to right and top to bottom). The eight panels show the evolution of the SOPs for different values of the longitudinal variable z. In the first stage of polarization attraction (panels 1–4, $z = 0$–2), all signal SOPs are contracted in the neighborhood of the two fixed points [green (light gray) points]. In the second stage (panels 5–8, $z = 2.5$ to $z = 4$), the SOPs follow the unstable manifolds to reach the final polarization attraction point. The blue (black), red (dark gray), and yellow (light gray) lines respectively depict the attraction line and the projection of a trajectory of the unstable manifold onto the Poincaré sphere. (The red color is associated with the $\vec{S}$ dynamics and the yellow one with the $\vec{J}$ dynamics.) The parameters are $\rho = 5$, $\vec{J}(L) = (1/\sqrt{3}, 1/\sqrt{3}, 1/\sqrt{3})$, and $L = 4$. A movie corresponding to this evolution is reported in the Supplemental Material [37]. The different quantities are dimensionless.

system around one of the two fixed points:

$$S_1 = \frac{\Delta}{3} + s_1;\ \ S_2 = s_2;\ \ J_1 = \frac{\Delta}{3} + j_1;\ J_2 = j_2. \tag{14}$$

We now determine the stable and unstable manifolds of the linearized dynamical system around such fixed points [33,34]. By linearizing the initial differential systems (3) and (4), we get the following relations:

$$\begin{aligned} \dot{s}_1 &= \alpha(s_2 + 2j_2) \\ \dot{s}_2 &= -\alpha(s_1 + 2j_1) \\ \dot{j}_1 &= -\alpha(j_2 + 2s_2) \\ \dot{j}_2 &= \alpha(j_1 + 2s_1), \end{aligned} \tag{15}$$

where $\alpha = \sqrt{1 - \Delta^2/9}$. We denote by M the 4×4 matrix:

$$M = \alpha \begin{pmatrix} 0 & 1 & 0 & 2 \\ -1 & 0 & -2 & 0 \\ 0 & -2 & 0 & -1 \\ 2 & 0 & 1 & 0 \end{pmatrix}.$$

The matrix M has two eigenvectors $\underline{u}_1^S = (-\sqrt{3}, -1, 0, 2)$, $\underline{u}_2^S = (-1, \sqrt{3}, 2, 0)$ with eigenvalue $-\sqrt{3}\alpha$, and two eigenvectors $\underline{u}_1^I = (\sqrt{3}, -1, 0, 2)$, $\underline{u}_2^I = (-1, -\sqrt{3}, 2, 0)$ with eigenvalue $\sqrt{3}\alpha$. In a neighborhood of the fixed points, a basis of the two-dimensional stable and unstable manifolds is given by the vectors $(\underline{u}_1^S, \underline{u}_2^S)$ and $(\underline{u}_1^I, \underline{u}_2^I)$, respectively. The unstable manifold can thus be parameterized by

$$\begin{bmatrix} s_1 \\ s_2 \\ j_1 \\ j_2 \end{bmatrix} = c_1 \underline{u}_1^I + c_2 \underline{u}_2^I.$$

We can represent the constants c_1 and c_2 in polar coordinates by

$$c_1 = R \sin\eta, \quad c_1 = R \cos\eta, \quad R = \sqrt{c_1^2 + c_2^2}, \quad \eta \in [0, 2\pi).$$

This leads explicitly to the representation

$$\begin{aligned} S_1 &= \frac{\Delta}{3} + R(\sqrt{3}\sin\eta - \cos\eta) \\ S_2 &= -R(\sin\eta + \sqrt{3}\cos\eta) \\ S_3 &= \sqrt{1 - S_1^2 - S_2^2} \\ J_1 &= \frac{\Delta}{3} + 2R\cos\eta \\ J_2 &= 2R\sin\eta \\ J_3 &= \sqrt{1 - J_1^2 - J_2^2} \end{aligned} \tag{16}$$

This shows that the linearized unstable manifold has the shape of a cone parameterized by R and η, with the fixed point at its vertex.

From Eqs. (16), we can express the parameters R, η in terms of J_1, J_2:

$$\begin{aligned} R &= \tfrac{1}{2}\sqrt{(J_1 - \Delta/3)^2 + J_2^2} \\ \sin\eta &= J_2/2R \\ \cos\eta &= (J_1 - \Delta/3)/2R. \end{aligned}$$

Inserting these equalities into Eqs. (16) and replacing $\sqrt{3}/2 = \sin(2\pi/3)$, $-1/2 = \cos(2\pi/3)$, we obtain the following relation between the coordinates $\vec{S}$ and $\vec{J}$ on the linearized unstable manifold:

$$\begin{aligned} S_1 &= \frac{\Delta}{2} + \cos\left(\frac{2\pi}{3}\right) J_1 + \sin\left(\frac{2\pi}{3}\right) J_2 \\ S_2 &= \frac{\Delta}{2\sqrt{3}} - \sin\left(\frac{2\pi}{3}\right) J_1 + \cos\left(\frac{2\pi}{3}\right) J_2 \\ S_3 &= \pm\sqrt{1 - S_1^2 - S_2^2}. \end{aligned} \tag{17}$$

Equations (17) yield an approximate analytical formula for the prediction of the polarization attraction. It is valid in particular for values of the pump $\vec{J}_L$ that are close enough to the fixed point, where the linearization gives a good approximation.

The parametrization (16) of the linearized unstable manifold gives the starting point for a numerical algorithm to determine the full (i.e., nonlinearized) unstable manifold. We choose a set of initial conditions on the unstable manifold using (16) with a small value of R and a set of values of the angle $\eta \in [0, 2\pi)$ and solve the system of differential equations (3) and (4). All the trajectories calculated in this way lay on the unstable manifold if R is small enough. This gives a method to predict the value of the polarization attraction $\vec{S}_L$ for an arbitrary pump $\vec{J}_L$. We scan the one parameter set of initial conditions η and integrate the differential equations (3) and (4) until we find an initial angle η_* and a z_* such that $\vec{J}(z_*) = \vec{J}_L$. The prediction is that the polarization of the signal will be attracted to the corresponding $\vec{S}(z_*)$. A result of this calculation is illustrated in Fig. 5.

We remark that, in the limit $\Delta = 0$, Eqs. (17) recover the standard coordinates of the attraction points (in both the linear and nonlinear cases) which define an equilateral triangle in the (S_1, S_2) plane with the pump SOP [12]. It is well known that in nonintegrable systems the stable manifold of one fixed point and the stable manifold of the other one generically have transverse intersections, while in integrable systems they merge into each other; in fact, they are the same manifold (see Ref. [24] and Appendix B for details). For large values of Δ, the transverse intersections of the stable and unstable manifolds can be expected to modify the behavior of the polarization attraction. This case, which goes beyond the scope of this paper, will be treated in a forthcoming work.

V. CONCLUSION AND PERSPECTIVES

We have proposed a general geometric approach to describe both in qualitative and quantitative ways a counterpropagating spatiotemporal wave dynamics in a medium of finite extension. This approach, based on the structure of the stationary Hamiltonian dynamics, provides a nontrivial generalization of the preceding works on this subject, because here the underlying stationary ODE system does not need to be integrable. More precisely, we have shown that the invariant sets of some particular fixed points of the stationary dynamics play a role of attraction for the PDE system. Such invariant manifolds can be viewed as a trace reminiscent of the singular tori which have been shown to exhibit a similar process of attraction in the integrable case [2]. The method developed here has been illustrated by considering the example of a weakly birefringent optical fiber.

We believe that this result is of significant potential interest in that it opens the door to a systematic investigation of the nonlinear dynamics of this type of counterpropagating PDE system, without requiring the severe constraint of integrability of the associated stationary Hamiltonian system. We recall in this respect that the Hamiltonian stationary dynamics of the system considered in this work is nonintegrable and chaotic, as it was discussed since the pioneering work [8]. On the basis of the numerical computations presented here, it seems crucial, however, that the Hamiltonian stationary dynamics is relatively close to integrability in order to observe the relaxation effect to a stationary state and the associated process of polarization attraction. This aspect needs to be confirmed by considering different examples of optical fiber systems, as well as different forms of nonlinear-wave systems, e.g., counterpropagating waves interacting in nonlinear periodic lattices [14]. In addition, we stress that the determination of the position and of the structure of the singular tori requires a heavy mathematical machinery, known as singular reduction theory [24]. This latter approach can hardly be applied to higher-dimensional dynamical systems, while the computation of the invariant sets can easily be performed for such systems, even in the integrable case. Work is in progress in order to address these issues. Finally, we would like to mention the possible nontrivial extension of the theoretical approach developed here to non-Hamiltonian systems, in particular, in relation to interesting studies in which repolarization phenomena based on the nonconservative Raman effect have been identified in optical fiber systems [38,39] (see also the recent work [40]).

APPENDIX A: DERIVATION OF THE DYNAMICAL EQUATIONS IN AN OPTICAL FIBER WITH A LOW BIREFRINGENCE

We derive the equations governing the propagation of the counterpropagating beams in the presence of a weak birefringence [8]. Starting from the Maxwell's equations and following the standard procedure [32], we obtained the following system of equations:

$$\begin{aligned} \frac{\partial E_x}{\partial t} + \nu \frac{\partial E_x}{\partial z} &= i\gamma \left\{ \left(|E_x|^2 + \frac{2}{3}|E_y|^2 \right) E_x \right. \\ &\quad + \frac{1}{3} E_y^2 E_x^* \exp[i 2\Delta z] \\ &\quad + \left(2|\bar{E}_x|^2 + \frac{2}{3}|\bar{E}_y|^2 \right) E_x \\ &\quad \left. + \frac{2}{3} E_y \bar{E}_y \bar{E}_x{}^* + \frac{2}{3} E_y \bar{E}_y{}^* \bar{E}_x \exp[i 2\Delta z] \right\}, \\ \frac{\partial E_y}{\partial t} + \nu \frac{\partial E_y}{\partial z} &= i\gamma \left\{ \left(|E_y|^2 + \frac{2}{3}|E_x|^2 \right) E_y \right. \\ &\quad + \frac{1}{3} E_x^2 E_y^* \exp[-i 2\Delta z] \end{aligned}$$

$$
\begin{aligned}
&+\left(2|\bar{E}_y|^2+\frac{2}{3}|\bar{E}_x|^2\right)E_y\\
&+\frac{2}{3}E_x\bar{E}_x\bar{E}_y{}^*+\frac{2}{3}E_x\bar{E}_x{}^*\bar{E}_y\exp[-i2\Delta z]\Big\},\\
\frac{\partial\bar{E}_x}{\partial t}-\nu\frac{\partial\bar{E}_x}{\partial z}&=i\gamma\Big\{\left(|\bar{E}_x|^2+\frac{2}{3}|\bar{E}_y|^2\right)\bar{E}_x\\
&+\frac{1}{3}\bar{E}_y{}^2\bar{E}_x{}^*\exp[i2\Delta z]\\
&+\left(2|E_x|^2+\frac{2}{3}|E_y|^2\right)\bar{E}_x\\
&+\frac{2}{3}\bar{E}_yE_yE_x^*+\frac{2}{3}\bar{E}_yE_y^*E_x\exp[i2\Delta z]\Big\}\\
\frac{\partial\bar{E}_y}{\partial t}-\nu\frac{\partial\bar{E}_y}{\partial z}&=i\gamma\Big\{\left(|\bar{E}_y|^2+\frac{2}{3}|\bar{E}_x|^2\right)\bar{E}_y\\
&+\frac{1}{3}\bar{E}_x{}^2\bar{E}_y{}^*\exp[-i2\Delta z]\\
&+\left(2|E_y|^2+\frac{2}{3}|E_x|^2\right)\bar{E}_y\\
&+\frac{2}{3}\bar{E}_xE_xE_y^*+\frac{2}{3}\bar{E}_xE_x^*E_y\exp[-i2\Delta z]\Big\},
\end{aligned}
\tag{A1}
$$

where (E_x,E_y) and $(\bar{E}_x,\bar{E}_y)$ are the components of the electric fields respectively associated with the signal and pump beams in the basis of rectilinear polarization, x and y being the principal axes of the fiber. The parameter $\Delta=k_x-k_y$ denotes the amount of birefringence, where $k_{x,y}$ are the wave vectors of the fields. Using the change of variables $E_x=A_x\exp[i\frac{\Delta}{2}z]$, $E_y=A_y\exp[-i\frac{\Delta}{2}z]$, $\bar{E}_x=\bar{A}_x\exp[-i\frac{\Delta}{2}z]$, and $\bar{E}_y=\bar{A}_y\exp[i\frac{\Delta}{2}z]$, the dynamical system can be written in terms of the A variables. If we then introduce the basis of circular polarizations defined by $u=\frac{(A_x+iA_y)}{\sqrt{2}}$, $v=\frac{(A_x-iA_y)}{\sqrt{2}}$, $\bar{u}=\frac{(\bar{A}_x+i\bar{A}_y)}{\sqrt{2}}$, and $\bar{v}=\frac{(\bar{A}_x-i\bar{A}_y)}{\sqrt{2}}$, the equations take the following form:

$$
\begin{aligned}
(\partial_t+\nu\partial_z)u&=\frac{2}{3}i\gamma[(|u|^2+2|v|^2+2|\bar{u}|^2+2|\bar{v}|^2)u\\
&\quad+2\bar{u}\bar{v}^*v]-i\frac{\Delta}{2}v,\\
(\partial_t+\nu\partial_z)v&=\frac{2}{3}i\gamma[(|v|^2+2|u|^2+2|\bar{u}|^2+2|\bar{v}|^2)v\\
&\quad+2\bar{v}\bar{u}^*u]-i\frac{\Delta}{2}u,\\
(\partial_t-\nu\partial_z)\bar{u}&=\frac{2}{3}i\gamma[(|\bar{u}|^2+2|v|^2+2|\bar{u}|^2+2|\bar{v}|^2)\bar{u}\\
&\quad+2uv^*\bar{v}]-i\frac{\Delta}{2}\bar{v},\\
(\partial_t-\nu\partial_z)\bar{v}&=\frac{2}{3}i\gamma[(|\bar{v}|^2+2|v|^2+2|\bar{u}|^2+2|\bar{v}|^2)\bar{v}\\
&\quad+2vu^*\bar{u}]-i\frac{\Delta}{2}\bar{u}.
\end{aligned}
\tag{A2}
$$

Now it proves convenient to introduce the Stokes coordinates defined by the relations

$$
\begin{aligned}
S_1&=i(u^*v-uv^*)\\
S_2&=u^*v+uv^*\\
S_3&=|u|^2-|v|^2\\
S_0^2&=(|u|^2+|v|^2)^2=\left(S_1^2+S_2^2+S_3^2\right)
\end{aligned}
\tag{A3}
$$

and

$$
\begin{aligned}
J_1&=i(\bar{u}^*\bar{v}-\bar{u}\bar{v}^*)\\
J_2&=\bar{u}^*\bar{v}+\bar{u}\bar{v}^*\\
J_3&=|\bar{u}|^2-|\bar{v}|^2\\
J_0^2&=(|\bar{u}|^2+|\bar{v}|^2)^2=\left(J_1^2+J_2^2+J_3^2\right).
\end{aligned}
\tag{A4}
$$

Next we normalize the problem with respect to the nonlinear time $\tau_0=1/(\Gamma J_0)$ and length $L_0=\nu\tau_0$, where $\Gamma=\frac{2}{3}\gamma$, i.e., the variables in physical units, can be recovered through the transformations $z\to zL_0$, $t\to t\tau_0$, $(S_i,J_i)\to(S_i,J_i)J_0$, and $\Delta\to\Delta L_0$. In dimensionless units, the Stokes variables are governed by the following equations:

$$
\begin{aligned}
(\partial_t+\partial_z)S_1&=S_3S_2+2S_3J_2\\
(\partial_t+\partial_z)S_2&=-S_3S_1-2S_3J_1+\Delta S_3\\
(\partial_t+\partial_z)S_3&=2J_1S_2-2S_1J_2-\Delta S_2
\end{aligned}
\tag{A5}
$$

and

$$
\begin{aligned}
(\partial_t-\partial_z)J_1&=J_3J_2+2J_3S_2\\
(\partial_t-\partial_z)J_2&=-J_3J_1-2J_3S_1+\Delta J_3\\
(\partial_t-\partial_z)J_3&=-2J_1S_2+2S_1J_2-\Delta J_2.
\end{aligned}
\tag{A6}
$$

APPENDIX B: STABLE AND UNSTABLE MANIFOLDS IN THE INTEGRABLE CASE $\Delta=0$

The analysis of the stationary solutions in the absence of birefringence ($\Delta=0$) has been studied from different perspectives in recent years [1,2,9]. Here, we describe the singular trajectories from the computation of the invariant sets so as to relate them with the analysis discussed above in the limit of vanishing birefringence. More precisely, we show that for $\Delta=0$, the full unstable manifold can be determined in explicit analytical form. Besides the Hamiltonian $H=2(S_1J_1+S_2J_2)-(S_3^2+J_3^2)/2$, there is a a second invariant $K=S_3-J_3$. The hyperbolic fixed points are at $S_3=1,J_3=1$ and at $S_3=-1,J_3=-1$. Thus the values of these two invariants on the stable and unstable manifolds are $H=-1$ and $K=0$. The invariant sets are determined by the system of equations

$$
\begin{aligned}
-1&=2(S_1J_1+S_2J_2)-\left(S_3^2+J_3^2\right)/2\\
S_3&=J_3.
\end{aligned}
$$

Inserting the second relation into the first one and using $S_3^2=1-S_1^2-S_2^2$, we obtain

$$
S_1^2+S_2^2+2(S_1J_1+S_2J_2)=0. \tag{B1}
$$

In order to find the solution $\vec{S}$ of this equation for a given $\vec{J}$, we use the spherical coordinates defined as follows:

$$
\begin{aligned}
J_1 &= \sqrt{1-J_3^2}\cos\varphi_J \\
J_2 &= \sqrt{1-J_3^2}\sin\varphi_J \\
S_1 &= \sqrt{1-J_3^2}\cos\varphi_S, \quad J_3 \in (-1,1), \\
S_2 &= \sqrt{1-J_3^2}\sin\varphi_S, \quad \varphi_J,\varphi_S \in [0,2\pi).
\end{aligned}
$$

Equation (B1) then becomes

$$
\left(1-J_3^2\right)[1+2\cos(\varphi_S-\varphi_J)] = 0, \tag{B2}
$$

which has the two solutions

$$
\varphi_S - \varphi_J = \pm\frac{2\pi}{3}. \tag{B3}
$$

The stable and unstable manifolds can therefore be described by

$$
\begin{aligned}
J_1 &= \sqrt{1-J_3^2}\cos\varphi_J \\
J_2 &= \sqrt{1-J_3^2}\sin\varphi_J \\
S_1 &= \sqrt{1-J_3^2}\cos\left(\varphi_J \pm \frac{2\pi}{3}\right) \\
S_2 &= \sqrt{1-J_3^2}\sin\left(\varphi_J \pm \frac{2\pi}{3}\right) \\
S_3 &= J_3,
\end{aligned}
$$

which can be rewritten as

$$
\begin{aligned}
S_1 &= \cos\left(\frac{2\pi}{3}\right)J_1 \pm \sin\left(\frac{2\pi}{3}\right)J_2 \\
S_2 &= \mp\sin\left(\frac{2\pi}{3}\right)J_1 + \cos\left(\frac{2\pi}{3}\right)J_2 \\
S_3 &= J_3.
\end{aligned} \tag{B4}
$$

This expression shows that the stable and unstable manifolds can be parameterized by the sphere $\vec{J}$. More precisely, they are a double cover of this sphere (because of the two signs $\pm$) that has two points of intersection at $J_3 = 1$ and $J_3 = -1$. These two isolated points of contact give the manifold the topology of a doubly pinched torus. The relations (B4) can be used to predict the polarization attraction: For each value of the pump $\vec{J}_L$, Eqs. (B4) give the two possible values of the signal $\vec{S}_L$ at the exit of the fiber. We remark that the structure of the exact stable and unstable manifolds (B4) of the integrable case is very close to that of the linearized nonintegrable model (17) in the vicinity of the fixed points. The only difference is a shift of the fixed points depending on the value of Δ.

The trajectories on the stable and unstable manifolds can be calculated explicitly for this model. Indeed, using the spherical coordinates, the equations of motion restricted to the stable and unstable manifolds can be written as

$$
\begin{aligned}
\frac{dJ_3}{dz} &= \pm\sqrt{3}\left(1-J_3^2\right) \\
\frac{d\cos\varphi_J}{dz} &= 0,
\end{aligned}
$$

and the solutions are

$$
\begin{aligned}
&J_3(z) = \pm\tanh[c_0 \pm \sqrt{3}(z-z_0)], \\
&c_0 = \operatorname{artanh} J_3(z_0) \\
&\varphi_J(z) = \varphi_J(z_0) = \text{constant} \\
&J_1(z) = \operatorname{sech}[c_0 \pm \sqrt{3}(z-z_0)]\cos(\varphi_J) \\
&J_2(z) = \operatorname{sech}[c_0 \pm \sqrt{3}(z-z_0)]\sin(\varphi_J) \\
&S_1(z) = \operatorname{sech}[c_0 \pm \sqrt{3}(z-z_0)]\cos\left(\varphi_J \pm \frac{2\pi}{3}\right) \\
&S_2(z) = \operatorname{sech}[c_0 \pm \sqrt{3}(z-z_0)]\sin\left(\varphi_J \pm \frac{2\pi}{3}\right) \\
&S_3(z) = J_3(z).
\end{aligned}
$$

The knowledge of these trajectories for the integrable case can be used to make more efficient the search of the attraction SOP for the nonintegrable model, at least for small values of Δ.

The fact that the equations for the full stable and unstable manifolds for the integrable model have the same structure as those for the linearized nonintegrable model can be explained by showing that the equations of motion of the integrable model restricted to the stable and unstable manifold can be transformed into linear equations. Indeed, they can be written as

$$
\begin{aligned}
\frac{dJ_3}{dz} &= \pm\sqrt{3}\left(1-J_3^2\right) \\
\frac{dJ_1}{dz} &= -J_3(J_2+2S_2) \\
\frac{dJ_2}{dz} &= J_3(J_1+2S_1) \\
\frac{dS_1}{dz} &= J_3(S_2+2J_2) \\
\frac{dS_2}{dz} &= -J_3(S_1+2J_1) \\
S_3 &= J_3.
\end{aligned}
$$

Making the change of variables $z' := \mp\int dz J_3(z)$, we obtain

$$
\begin{aligned}
\frac{dJ_1}{dz'} &= (J_2+2S_2) \\
\frac{dJ_2}{dz'} &= -(J_1+2S_1) \\
\frac{dS_1}{dz'} &= -(S_2+2J_2) \\
\frac{dS_2}{dz'} &= (S_1+2J_1),
\end{aligned}
$$

which have exactly the same form as the linearized equations (15).

[1] D. David, D. D. Holm, and M. V. Tratnik, Phys. Rep. **187**, 281 (1990).
[2] E. Assémat, A. Picozzi, H.-R. Jauslin, and D. Sugny, J. Opt. Soc. Am. B **29**, 559 (2012).
[3] G. Millot and S. Wabnitz, J. Opt. Soc. Am. B **31**, 2754 (2014).
[4] J. Yumoto and K. Otsuka, Phys. Rev. Lett. **54**, 1806 (1985).
[5] G. Gregori and S. Wabnitz, Phys. Rev. Lett. **56**, 600 (1986).
[6] S. Wabnitz and G. Gregori, Opt. Commun. **59**, 72 (1986).
[7] V. E. Zakharov and A. V. Mikhailov, JETP Lett. **45**, 279 (1987).
[8] S. Trillo and S. Wabnitz, Phys. Rev. A **36**, 3881 (1987).
[9] S. Pitois, A. Picozzi, G. Millot, H. R. Jauslin, and M. Haelterman, Europhys. Lett. **70**, 88 (2005).
[10] S. Pitois, G. Millot, and S. Wabnitz, Phys. Rev. Lett. **81**, 1409 (1998).
[11] S. Pitois, J. Fatome, and G. Millot, Opt. Express **16**, 6646 (2008).
[12] E. Assémat, S. Lagrange, A. Picozzi, H. R. Jauslin, and D. Sugny, Opt. Lett. **35**, 2025 (2010).
[13] V. V. Kozlov and S. Wabnitz, Opt. Lett. **35**, 3949 (2010).
[14] D. Sugny, A. Picozzi, S. Lagrange, and H. R. Jauslin, Phys. Rev. Lett. **103**, 034102 (2009).
[15] S. Lagrange, D. Sugny, A. Picozzi, and H. R. Jauslin, Phys. Rev. E **81**, 016202 (2010).
[16] E. Assémat, D. Dargent, A. Picozzi, H. R. Jauslin, and D. Sugny, Opt. Lett. **36**, 4038 (2011).
[17] M. Grenier, H.-R. Jauslin, C. Klein, and V. B. Matveev, J. Math. Phys. **52**, 082704 (2011).
[18] S. Wabnitz, Opt. Lett. **34**, 908 (2009).
[19] M. Guasoni, E. Assémat, P. Morin, A. Picozzi, J. Fatome, S. Pitois, H. Jauslin, G. Millot, and D. Sugny, J. Opt. Soc. Am. B **31**, 572 (2014).
[20] J. Fatome, S. Pitois, P. Morin, and G. Millot, Opt. Express **18**, 15311 (2010).
[21] V. V. Kozlov, J. Nuno, and S. Wabnitz, J. Opt. Soc. Am. B **28**, 100 (2011).
[22] M. Barozzi and A. Vannucci, Photonics Res. **3**, 229 (2015).
[23] K. Turitsyn and S. Wabnitz, Opt. Commun. **307**, 62 (2013).
[24] R. H. Cushman and L. M. Bates, *Global Aspects of Classical Integrable Systems* (Birkhäuser, Berlin, 1997).
[25] K. Efstathiou, *Metamorphoses of Hamiltonian Systems with Symmetry*, Lecture Notes in Mathematics Vol. 1864 (Springer-Verlag, Heidelberg, 2004).
[26] P.-Y. Bony, M. Guasoni, E. Assémat, S. Pitois, D. Sugny, A. Picozzi, H. R. Jauslin, and J. Fatome, J. Opt. Soc. Am. B **30**, 2318 (2013).
[27] P.-Y. Bony, M. Guasoni, P. Morin, D. Sugny, A. Picozzi, H.-R. Jauslin, S. Pitois, and J. Fatome, Nat. Commun. **5**, 4678 (2014).
[28] J. Fatome, S. Pitois, P. Morin, E. Assémat, D. Sugny, A. Picozzi, H.-R. Jauslin, G. Millot, V. Kozlov, and S. Wabnitz, Sci. Rep. **2**, 938 (2012).
[29] E. Heebner, R. S. Bennink, R. W. Boyd, and R. A. Fisher, Opt. Lett. **25**, 257 (2000).
[30] A. Picozzi *et al.*, Phys. Rep. **542**, 1 (2014).
[31] M. Barozzi and A. Vannucci, J. Opt. Soc. Am. B **31**, 2712 (2014).
[32] Y. S. Kivshar and G. P. Agrawal, *Optical Solitons: From Fibers to Photonics Crystals* (Academic Press, New York, 2003).
[33] V. I. Arnol'd, *Mathematical Methods of Classical Mechanics* (Springer-Verlag, New York, 1989).
[34] S. Wiggins, *Global Bifurcations and Chaos* (Springer Verlag, New York, 1988).
[35] B. Rink, Nonlinearity **17**, 347 (2004).
[36] H. Broer, R. Cushman, F. Fasso, and F. Takens, Ergod. Theor. Dyn. Syst. **27**, 725 (2007).
[37] See Supplemental Material at http://link.aps.org/supplemental/10.1103/PhysRevA.93.053830 for a video about the polarization attraction phenomenon.
[38] S. Pitois, A. Sauter, and G. Millot, Opt. Lett. **29**, 599 (2004).
[39] V. V. Kozlov, J. Nuno, J. D. Ania-Castanon, and S. Wabnitz, Opt. Lett. **35**, 3970 (2010).
[40] V. Kalashnikov, S. V. Sergeyev, G. Jacobsen, S. Popov, and S. K. Turitsyn, Light: Sci. Appl. **5**, e16011 (2016).